POLISH MARITIME RESEARCH 2 (118) 2023 Vol. 30; pp. 95-104
10.2478/pomr-2023-0025

ENERGY MANAGEMENT STRATEGY CONSIDERING ENERGY STORAGE SYSTEM DEGRADATION FOR HYDROGEN FUEL CELL SHIP

Wei Cao[1]
Pan Geng[1]
Xiaoyan Xu[1]
Tomasz Tarasiuk[2]*
[1] Shanghai Maritime University, Logistics Engineering College, China
[2] Gdynia Maritime University, Poland

* Corresponding author: *t.tarasiuk@we.umg.edu.pl (Tomasz Tarasiuk)*

ABSTRACT

A hybrid energy system (HES) including hydrogen fuel cell systems (FCS) and a lithium-ion (Li-ion) battery energy storage system (ESS) is established for hydrogen fuel cell ships to follow fast load transients. An energy management strategy (EMS) with hierarchical control is presented to achieve proper distribution of load power and enhance system stability. In the high-control loop, a power distribution mechanism based on a particle swarm optimization algorithm (PSO) with an equivalent consumption minimization strategy (ECMS) is proposed. In the low-level control loop, an adaptive fuzzy PID controller is developed, which can quickly restore the system to a stable state by adjusting the PID parameters in real time. Compared with the rule-based EMS, hydrogen consumption is reduced by 5.319%, and the stability of the power system is significantly improved. In addition, the ESS degradation model is developed to assess its state of health (SOH). The ESS capacity loss is reduced by 2% and the daily operating cost of the ship is reduced by 1.7% compared with the PSO-ECMS without considering the ESS degradation.

Keywords: Hydrogen fuel cell ship, Energy management, Fuzzy PID, Equivalent energy consumption minimum, Energy storage system degradation

INTRODUCTION

The data show that international shipping released about 796 million tons of CO_2 in 2012. As a result, the International Maritime Organization has developed regulations to reduce CO_2 emissions from ships [1, 2]. Therefore, all-electric ships with fuel cells and energy storage systems have gained great attention in various countries due to their high efficiency, but chiefly their pollution-free characteristics have to be underlined [3]. Hydrogen fuel cells are now widely used in the fuel cell vehicle industry, but their application in the marine industry is still in its infancy. However, this trend is expected to grow in the future [4].

The power distribution mechanism is the core part of the HES, and can coordinate the output power of power sources and improve power system stability. Intelligent algorithms such as the sine and cosine algorithm, model predictive control, and deep reinforcement learning algorithm are being implemented to achieve a reasonable distribution of the load power among different power sources. For example, Mehdi et al. [5] developed a zero-emission ship model with FCS, Li-ion batteries, as well as shore power, in addition to proposing an EMS based on an improved sine and cosine algorithm. The objective is to reduce hydrogen consumption and prolong the lifetime of the power sources. In [6], the authors proposed a controller consisting of an intelligent algorithm, filters,

and state logic control for a ship with a gas turbine, battery, and supercapacitors (SUC) to achieve real-time control. In [7, 8], a multi-objective deep reinforcement learning-based algorithm is presented for an emission-free ship to optimize the load power allocation among the FCS and ESS. In [9], the authors developed a nonlinear ship model considering the sea state and weather, with the model predictive control being used to solve the optimization problem. In [10], the authors argue that the parameters of the hybrid ESS are critical for the power system. So recursive least squares are applied for online parameter identification and the model predictive control is used to share the load power between the battery and SUC. In [11], the output power of the FCS and battery is determined by minimizing the operation cost. In [12], to reduce the ESS capacity loss, a deep reinforcement learning algorithm is used to jointly optimize the ESS sizing and power distribution mechanism.

The control methods of DC/DC converters have been optimized to improve the stability of the power system. In [13], the authors proposed a controller for DC/DC converters based on a sliding mode control and PI control to minimize bus voltage fluctuations. In [14], a bus voltage control method based on drop control is proposed. This method solves the voltage drop by adding the voltage correction value to the reference voltage. In [15], the authors present an adaptive fuzzy logic controller, and it can be adapted to different operation conditions by adjusting the parameters in real time.

For ship power systems, the EMS consists of two key aspects: the power distribution mechanism and the controller for the DC/DC converter; however, most articles focus on one aspect alone and ignore the impact of ESS degradation on the power system. Therefore, an EMS with hierarchical control is proposed in this paper.

STRUCTURE AND MODEL OF FUEL CELL SHIP

POWER SYSTEM STRUCTURE

For the article purpose, the conventional radial distribution architecture is considered. It is assumed that the system consists of 2×135 kW hydrogen FCS, 2×550 V/100Ah ESS, which can be currently bought on the market, completed by converters, control units, propulsion load, and hotel load. The topology of the analyzed shipboard power system (SPS) is shown in Fig. 1. As the FCS suffers from a slow dynamic response, it requires a couple with ESS, which is applied for covering the fast load variations [16]. During the period of high load power, to meet the load power requirement, the output power of the FCS and ESS is greater than zero. During the period of low load power, the ESS absorbs excess energy to maintain the bus voltage stability [17]. During the entire operation, the ESS has two states, charging and discharging. It is connected to a boost/buck DC/DC converter. Since the FCS does not absorb energy from the system, it is connected to a boost DC/DC converter.

According to the FCS data, when the rated power of the fuel cell system is 135kW, the optimal output power during operation is in the range of 27 kW-120 kW. Both low and high operating conditions will cause incomplete chemical reactions and subsequent damage to the reactor, resulting in a shortened lifetime. Therefore, for subsequent analyses the minimum output power of the fuel cell system is set to 27kW.

The energy storage system (ESS) is to account for the fast load variation. For subsequent analyses, it was assumed that the peak load will equal to 110 kW and single ESS should meet this demand. Therefore, according to recommendation ref. [18], the nominal energy of single ESS was set to 55 kWh.

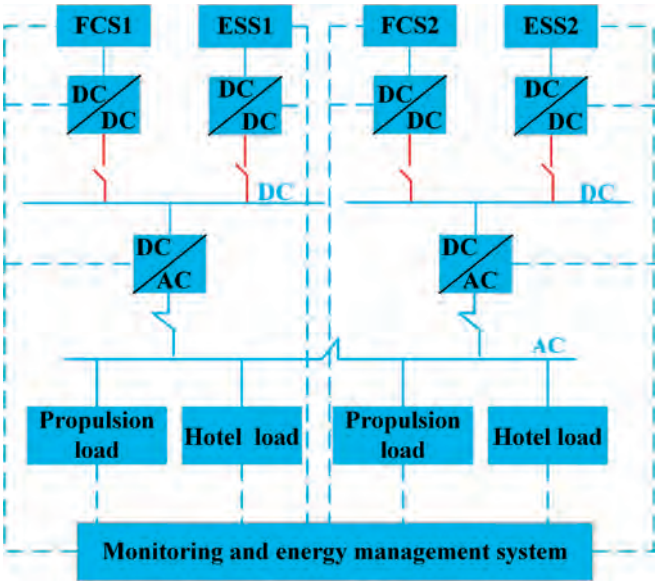

Fig. 1. The topology of the SPS

FC model

The equivalent circuit of a fuel cell (FC) is shown in Fig. 2 and the expression of the fuel cell output voltage is shown in Eq. (1) [19].

$$V_{fc} = E_{oc} - NAln\left(\frac{i_{fc}}{i_0}\right) \times \frac{3}{sT_d+3} - (R_{ohm} \times i_{fc}) \quad (1)$$

where V_{fc} and i_{fc} are the output voltage and output current of the fuel cell respectively. E_{oc} is the open circuit voltage, N is the number of cells, T_d is the response time and R_{ohm} represents the internal resistance.

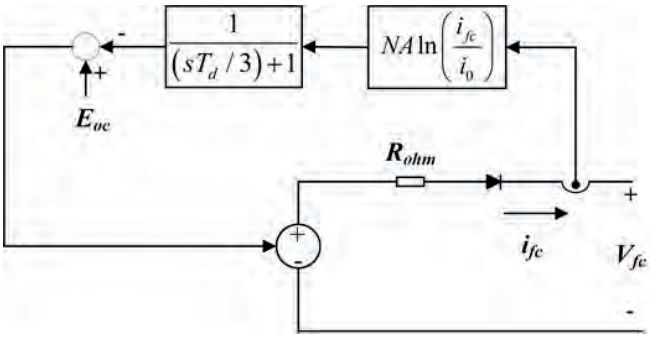

Fig. 2. The equivalent circuit of a fuel cell stack

Li-ion battery model

The dynamic feature of the Li-ion battery is represented by the Thevenin model as shown in Fig 3. The terminal voltage of the battery is shown in Eq. (2) [20].

$$\begin{cases} C\frac{d}{dt}U_C = i_B - \frac{U_C}{R_2} \\ U_B = U_{OC} - (U_C + i_B R_1) \end{cases} \quad (2)$$

where R_1 is the ohmic resistance, R_2 is the polarization resistance, U_C is the polarization voltage. U_B and i_B are the output voltage and output current of the Li-ion battery, U_{oc} is the open circuit voltage of the Li-ion battery.

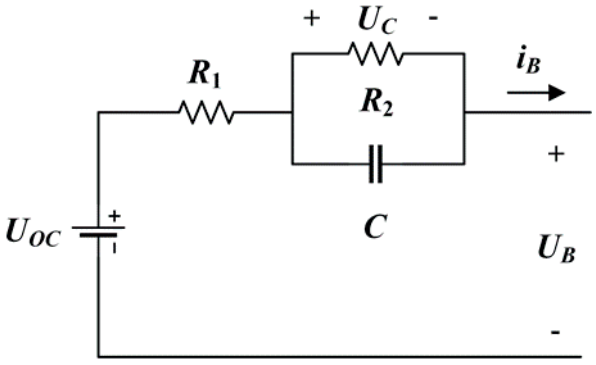

Fig 3. Thevenin model

THE ESS DEGRADATION MODEL

The methods for assessing the SOH include physical model-based methods, semi-empirical life models, and data-driven methods [21]. The ESS must be replaced when its actual capacity is 80% of the rated capacity. The semi-empirical long-term cycle life model is developed in [22]. In this paper, an ESS degradation model based on the semi-empirical life model is developed to calculate the loss of ESS capacity.

$$Q_{loss} = m\sum_{i=1}^{N}[q(i)]^{0.554} \times e^{(-\frac{E}{RT})} \quad (3)$$

$$\begin{cases} q = |I_{ESS}| \times t \\ I_{ESS} = \frac{P_{ESS}}{U_{ESSnom}} \end{cases} \quad (4)$$

$$ESS_{int} = C_{power} \times P_{rate} + C_{capacity} \times Q_{rate}$$
$$C_{loss} = ESS_{int} \times (\frac{Q_{loss}}{0.2}) \quad (5)$$

where m is a constant, E is the activation energy, and both of them are linearly related to the current rate (C_{rate}). R is the gas constant. It is assumed that the operating voltage of the ESS is stable at the rated value and the temperature (T) is kept constant during the operation, q is the amount of charge absorbed and released by the ESS per unit of time. C_{power} is the cost per unit power of the ESS ($200/kW). $C_{capacity}$ is the cost per unit capacity of the ESS ($125/kWh). C_{loss} is the ESS capacity loss cost. ESS_{int} is the installation cost of the ESS. The values of the parameters are listed in Table 1 [23].

Tab. 1. The parameters for ESS degradation model

Parameter	Value
C_{rate}	2C
m	19300
E	-31000
R	8.31 J/mol/K
T	25°C

ENERGY MANAGEMENT STRATEGY

The EMS with hierarchical control presented in this paper involves two layers of control loops: the high-level control loop realizes the reasonable distribution of load power between different power sources depending on the load power and the state of charge (SOC) of the ESS; the low-level control loop suppresses power system fluctuations by controlling the DC/DC converter. The overall structure diagram is shown in Fig. 4.

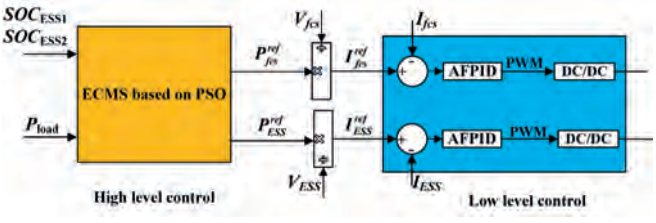

Fig. 4. Hierarchical control structure

HIGH-LEVEL CONTROL

In the high-level control loop, two power distribution mechanisms are designed:

(i) A power allocation mechanism based on the Support Vector Machine (SVM); (ii) An equivalent consumption minimization strategy (ECMS) based on PSO.

The core idea of the ECMS is to equate the energy demand of the ESS with the same amount of hydrogen consumption, which is regarded as indirect hydrogen consumption. The energy demand of the hydrogen FCS is direct hydrogen consumption. The model is solved to minimize the total hydrogen consumption [24]. The algorithm flow chart of the PSO-ECMS is shown in Fig. 5. The instantaneous hydrogen consumption can be defined as the following formula:

$$\begin{cases} minJ_{H_2,eqv}(t) = C_{price} \times \sum_{i=1}^{2} \left(m_{fcsi}(t) + m_{ESSi}(t) \right) \\ m_{fcsi}(t) = \frac{P_{fcsi}(t)}{LHV \eta_{fcs}(t)} \\ \eta_{fcs} = (-0.1123 \times P_{fcs} + 54.1)/100 \\ m_{ESSi}(t) = \frac{n(t)}{LHV} P_{ESSi}(t) p(SOC) \end{cases} \quad (6)$$

where C_{price} is the price of hydrogen ($4.5/kg); n(t) is the equivalence factor, which serves to convert the electrical energy consumed by the ESS into an equivalent amount of hydrogen consumption, $p(SOC)$ is the penalty factor, which is used to ensure that the SOC remains in a specific range. $\eta_{fcs}(t)$ is the efficiency of the FCS at time t, the relationship between the output power and efficiency of the FCS is shown in Fig. 6. P_{fcs}(t) is the output power of the hydrogen FCS at time t; LHV is the low heat value of hydrogen (120MJ/kg); P_{ESS}(t) is the output power of the ESS at time t.

$$\mathrm{n(t)} = 1 - 2\mu \times \left[\frac{SOC(t)}{SOC_{max} + SOC_{min}} - 0.5 \right] \quad (7)$$

$$\mathrm{p(SOC)} = 1 - \left[\frac{SOC(t) - SOC_{target}}{SOC_{max} - SOC_{min}} \right]^3 \quad (8)$$

where μ is the equilibrium coefficient; SOC_{max}, SOC_{target}, and SOC_{min} are the maximum, target, and minimum values of the SOC respectively. When $SOC > SOC_{target}$ and $p(SOC) < 1$, the cost of ESS energy is lower and the ESS is biased towards discharge; when $SOC > SOC_{target}$ and $p(SOC) > 1$, the cost of ESS energy increases and the ESS is biased towards charging.

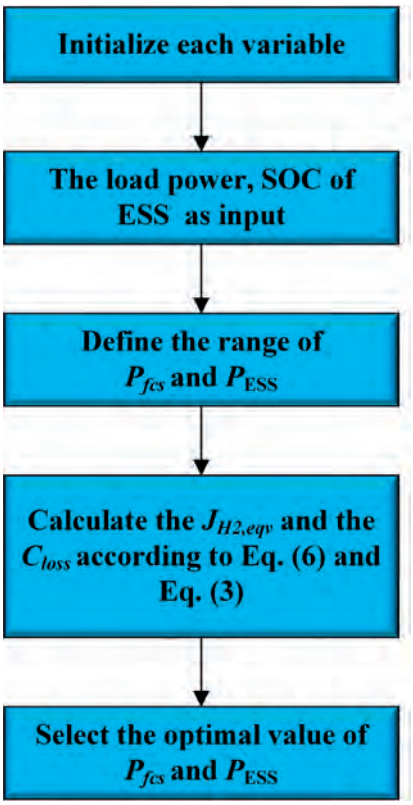

Fig. 5. The flowchart for PSO-ECMS

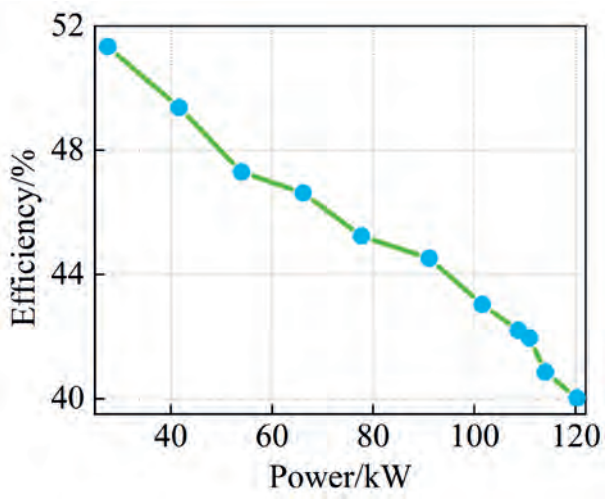

Fig .6. The relationship between the output power and efficiency of the FCS

The following equation about the SOC of the ESS must be satisfied:

$$30\% \leq \mathrm{SOC} \leq 90\% \quad (9)$$

The following equation about P_{fcs} must be satisfied:

$$\mathrm{P}_{fcs,min} \leq P_{fcs} \leq \mathrm{P}_{fcs,max} \quad (10)$$

The following equation about P_{ESS} must be satisfied:

$$|P_{ESS}| \leq P_{ESS,max} \quad (11)$$

The change rate of the FCS output power must satisfy Eq. (12):

$$\left|P_{fcs}(t+1) - P_{fcs}(t)\right| \leq \triangle P_{fcs,max} \quad (12)$$

The power system must maintain a real-time power balance:

$$P_{load} = \sum_i^2 \left(\eta_{DC1} P_{fcsi} + \eta_{DC2} \max(P_{ESSi}, 0) + \frac{1}{\eta_{DC2}} \min(P_{ESSi}, 0)\right) \quad (13)$$

where η_{DC1} is the efficiency of the boost DC/DC converter (0.98); η_{DC2} is the efficiency of the boost/buck DC/DC converter (0.9).

The principle of the SVM is to define the reference value of the output power of the FCS and ESS based on the SOC of the ESS and load power. In this paper, the SOC is divided into three stages, and the power distribution mechanism is shown in Fig. 7.

The total output power of ESS is obtained according to Eq. (14).

$$P_{ESS} = P_{load} - P_{fcs1,ref} - P_{fcs2,ref} \quad (14)$$

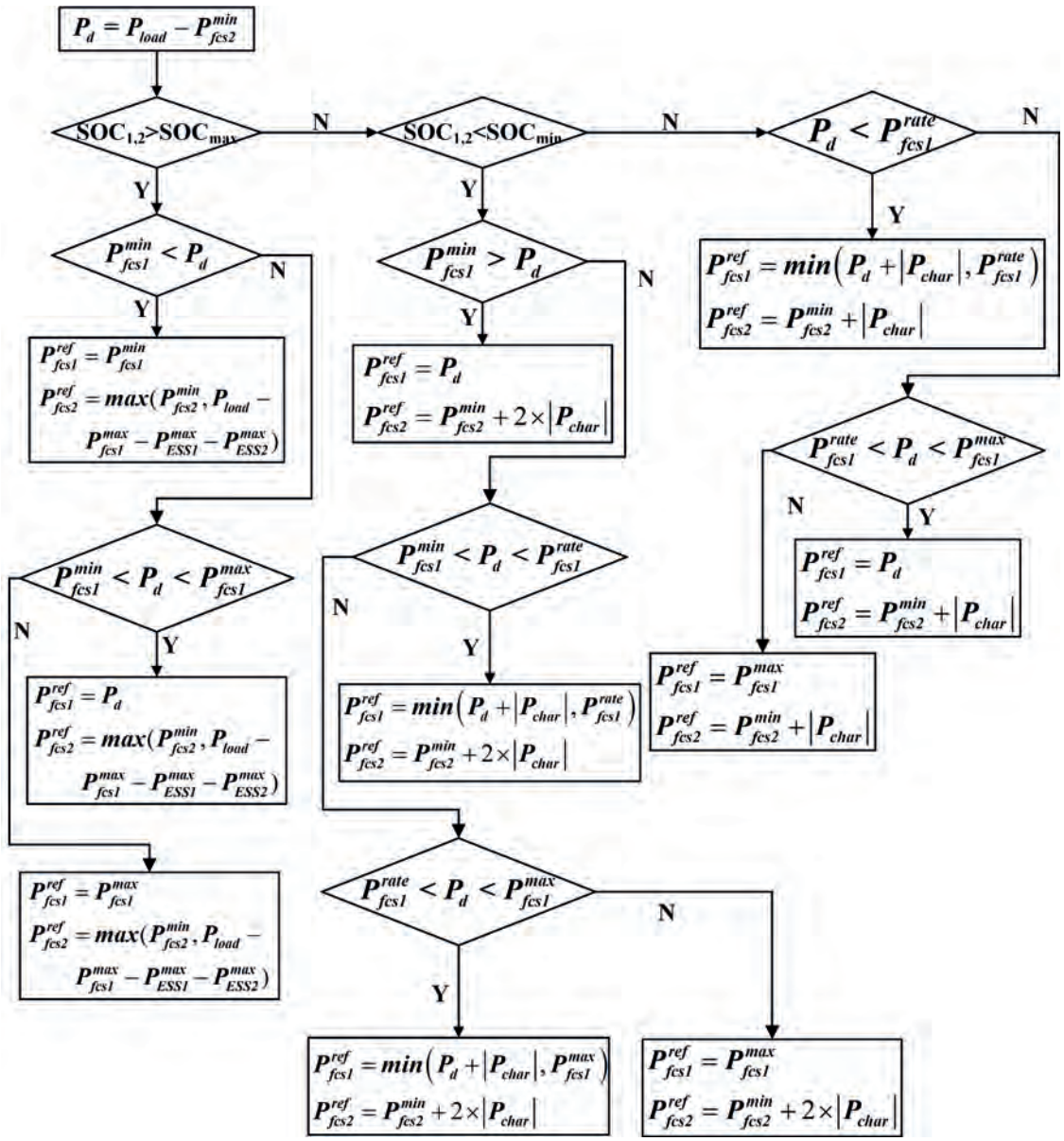

Fig. 7. Power distribution mechanism based on SVM

The output power of ESS1 and ESS2 are determined according to Eq. (15) and Eq. (16).

$$P_{ESS1,ref} = \begin{cases} \frac{SOC_1}{SOC_1+SOC_2} \times P_{ESS}, P_{ESS} > 0 \\ \frac{|SOC_1-SOC_{target}|}{|SOC_1-SOC_{target}|+|SOC_2-SOC_{target}|} \times P_{ESS}, P_{ESS} < 0 \end{cases} \quad (15)$$

$$P_{ESS2,ref} = = \begin{cases} \frac{SOC_2}{SOC_1+SOC_2} \times P_{ESS}, P_{ESS} > 0 \\ \frac{|SOC_2-SOC_{target}|}{|SOC_1-SOC_{target}|+|SOC_2-SOC_{target}|} \times P_{ESS}, P_{ESS} < 0 \end{cases} \quad (16)$$

LOW-LEVEL CONTROL

An adaptive fuzzy PID controller (AFPID) is presented in this paper by combining fuzzy control with PID control. The structure of the AFPID is shown in Fig. 8. The AFPID takes the error and the rate of change of the error as input, and corrects the control parameters of the PID in real time by fuzzification, fuzzy inference machine, and defuzzification so that the controller has good dynamic and static characteristics. The fuzzy domains of the variables and the values of the quantization factors are summarized in Table 2.

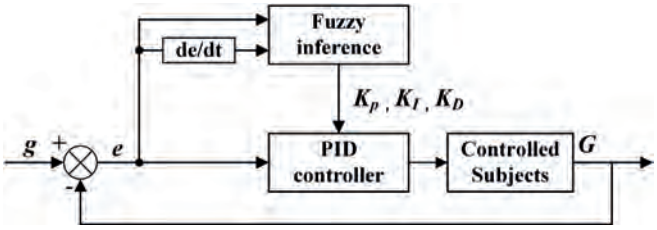

Fig. 8. AFPID controller

Tab. 2. The parameters for AFPID

	e	ec	ΔK_P	ΔK_I	ΔK_D
Fuzzy domains	[-2,6]	[-4,4]	[0,6]	[6,12]	[0,6]
Quantization factors	0.05	0.01	29	30	5
Affiliation function	Triangles	Triangles	NB/PB is Gaussian, the rest is triangular	Triangles	Triangles

RESULT

The EMS with hierarchical control is verified using Matlab/Simulink software, and the main parameters of the model are shown in Table 3.

For further analyses, authors assumed that the considered load profile would correspond to the load profile registered onboard of the hydrogen fuel cell passenger ship "Alsterwasser" [25]. There are four operation states during the voyage, namely, cruising, docking, anchoring and sailing (accelerating). However, this paper focuses on the effect of load fluctuation on the ship power system, so only the docking and sailing are considered, when the high load variations and peak values are observed. The load profiles for the considered states are shown in Fig. 9 [25]. According to the ship operation profile, there are ten such states during one hour. For anchoring state the load is low and for cruising it is constant, more or less 40 kW. Finally, during the docking phase, the load power fluctuates in a wide range, and the peak load power reaches a maximum during the sailing phase.

Tab. 3. The main parameters of the model

	Parameter	Value
FCS	$P_{fcs,min}$	27 kW
	$P_{fcs,max}$	137.5 kW
	$P_{fcs,rate}$	135 kW
	Power ramp rate limit of FCS	±4.24 kW/s
ESS	Nominal voltage/capacity	550V/100Ah
	$P_{ESS,max}$	110 kW
	SOC_{max}	100%
	SOC_{min}	30%
	SOC_{target}	80%

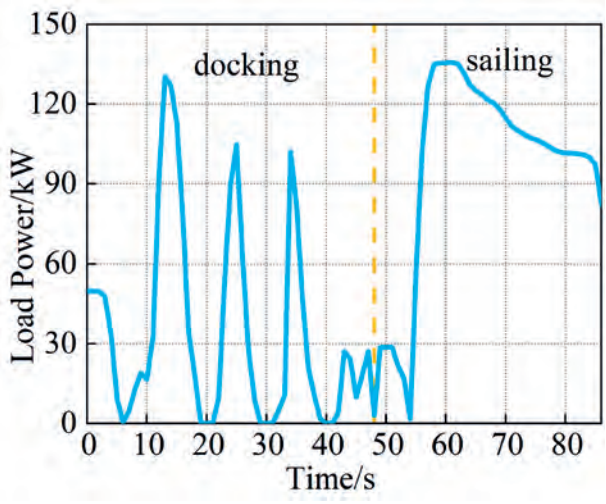

Fig. 9. Load profile

COMPARISON OF THE DIFFERENT POWER DISTRIBUTION MECHANISMS

SVM

The output power of the power sources and the SOC of the ESS are shown in Fig. 10. Fig. 10(a) and Fig. 10(b) indicate that the output power of FCS1 fluctuates greatly since the SVM fails to consider the characteristics of the hydrogen FCS, which will reduce its lifetime. The load power does not exceed the maximum output power of FCS1, ESS1, and ESS2, so during the entire operation the FCS2 works with constant output power of 27 kW, according to control (Fig. 7). Finally, the energies provided by FCS1 and FCS2 are 1.1 kWh and 0.65 kWh, respectively.

The initial values of the SOC of ESS1 and ESS2 are the same, so the output power curves of ESS1 and ESS2 are the same. The average output power of ESS1 and ESS2 is smaller during the entire operation. The results indicate that the power distribution mechanisms based on SVM do not consider the characteristics of each power source and cannot achieve optimal power distribution. When the output power of the ESS is greater than zero, it implies a release of energy and vice versa. From Fig. 10(c), the SOC of ESS1 and ESS2 fluctuates within the bounded range and the final SOC of ESS1 and ESS2 is 79.52%.

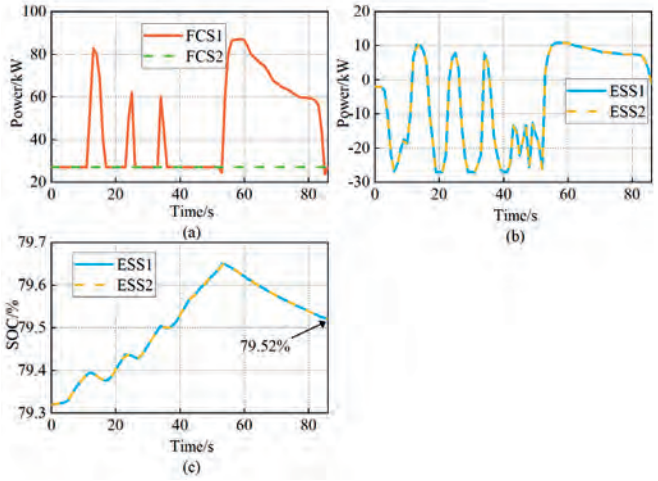

Fig. 10. (a) FCS output power; (b) ESS output power; (c) SOC of the ESS

PSO-ECMS without considering ESS degradation

The output power of the power sources and the SOC of the ESS are shown in Fig. 11. From Fig. 11(a), FCS1 and FCS2 operate in the highest efficiency range and the output power does not fluctuate greatly over the entire operation. During the docking phase, the PSO-ECMS can control the rate of change of the FCS output power, so the output power curve of the FCS is smoother and the peak output power of FCS1 reduces by 50.6% compared with SVM, which can prolong the lifetime of the FCS. From Fig. 11(b), due to the ESSs being used to track the fast load variations, the output power of ESS1 and ESS2 fluctuate greatly during the operation. Fig. 11(c) shows that, during the docking phase, the load power is lower. During this period, ESS1 and ESS2 are charging for more periods, so the SOC reaches the maximum value after the docking phase ends. During the sailing phase, the load power reaches its maximum, and the output power of ESS1 as well as ESS2 reaches peak values. Therefore, the SOC keeps falling. The final SOC of ESS1 and ESS2 is 79.5% and 79.38%, respectively. Both of these values are close to the target SOC.

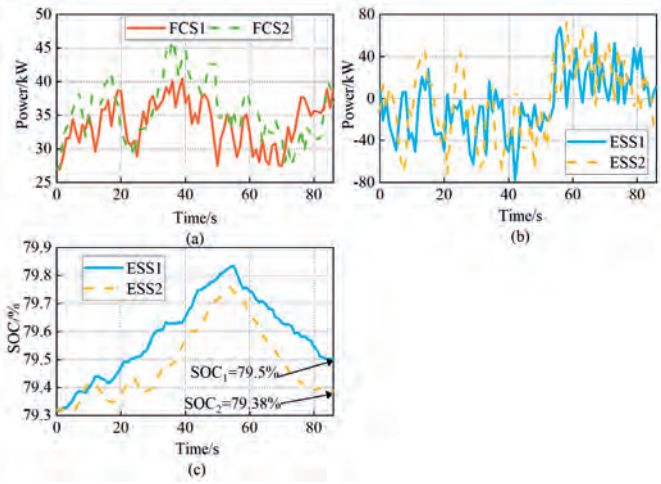

Fig. 11. (a) FCS output power; (b) ESS output power; (c) SOC of the ESS

PSO-ECMS considering ESS degradation

The loss of ESS capacity is calculated based on its output power. From Fig. 12(a) and Fig. 12(b), it is clear that, although the output power of FCS1 and FCS2 does not fluctuate greatly when considering the ESS degradation, it has been rising slowly to reduce the output power of the ESS. Hence, the average output power of the FCS is higher compared with PSO-ECMS when ESS degradation is not considered. From Fig. 12(c), during the docking phase, the ESS SOC keeps increasing. However, during the sailing phase, the SOC of the ESS is smoother. This indicates that the output power of the ESS is smaller, which can reduce the ESS capacity loss. The SOC fluctuates within a reasonable range and the final SOC of ESS1 and ESS2 is 79.8% and 79.63%, respectively. Both of them are approximated target values.

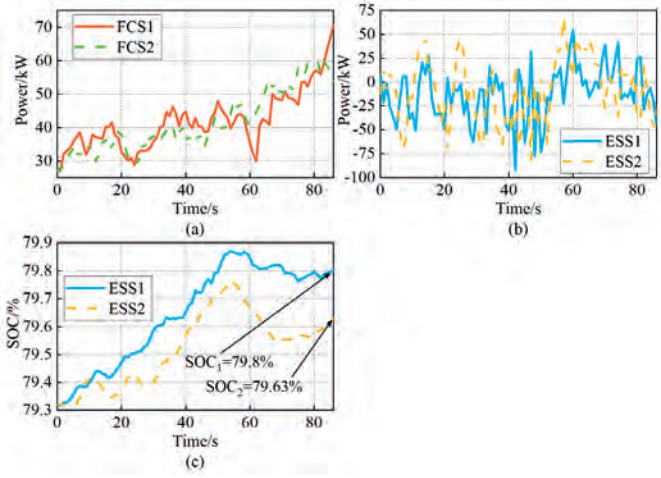

Fig. 12. (a) FCS output power; (b) ESS output power; (c) SOC of the ESS

The hydrogen consumption

Fig. 13(a) indicates the hydrogen consumption increase since the SVM-based power allocation mechanism is an empirical rule-based approach. Although hydrogen consumption is lower during some periods, it cannot achieve the global optimum. The hydrogen consumption is 101.7 g in one cycle and the operation cost is $0.45765 with SVM. From Fig. 13(b), the PSO-ECMS-based power allocation mechanism makes the hydrogen FCSs feed the remaining energy back to the ESS during the docking phase, so the instantaneous hydrogen consumption is higher in some periods. During the sailing phase, the energy stored in the ESS is effectively utilized, and the instantaneous hydrogen consumption is low. Without considering ESS degradation, the hydrogen consumption is 96.29 g in one cycle and the operation cost is $0.4333 with the PSO-ECMS. Compared with SVM, the operation cost reduces by 5.319%. Fig. 13(c) indicates that the hydrogen consumption is 99.63 g in one cycle and the operation cost is $0.44833 with the PSO-ECMS when considering the ESS degradation. Compared with SVM, the operation cost reduces by 2%.

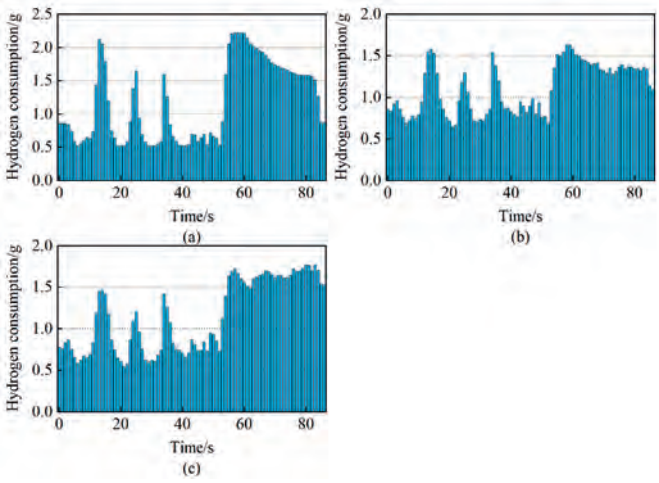

Fig. 13. (a) Hydrogen consumption of SVM; (b) Hydrogen consumption with PSO-ECMS without considering ESS degradation; (c) Hydrogen consumption with PSO-ECMS considering ESS degradation

ESS degradation

From Fig. 14(a), the total capacity loss is 0.00883% in one cycle without considering ESS degradation. From Fig. 14(b), when the ESS degradation constraint is considered, the output power of the ESS is reduced and the total capacity loss of the ESS is 0.00866% in one cycle. The capacity loss is reduced by 2% compared to that without considering ESS degradation. The hydrogen consumption is $0.4333 and the cost of the ESS capacity loss is $12.74 without considering ESS degradation. However, when ESS degradation is taken into account, the hydrogen consumption is $0.44833 and the cost of the ESS capacity loss is $12.5, with the daily operation cost being reduced by 1.7%.

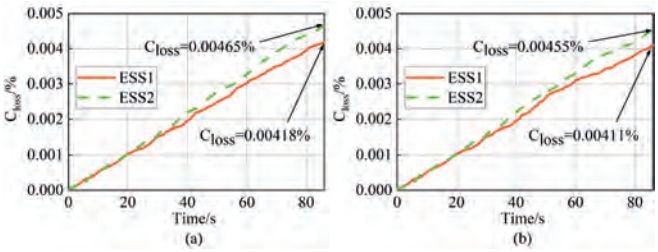

Fig. 14. (a) The ESS capacity loss without considering ESS degradation; (b) The ESS capacity loss considering ESS degradation

Bus voltage

The fluctuation curve of the bus voltage on the DC side of the ship power system is shown in Fig. 15. From Fig. 15(a), it can be observed that the AFPID controller makes the bus voltage fluctuations smaller and closer to the desired value. Fig. 15(b) shows that the deviation of the bus voltage from the reference value is reduced by 7.22% compared to PID control by between 10s and 30s. The result shows that the bus voltage is smoother and the stability of the ship power system is significantly improved when AFPID control is used for the low-level control loop.

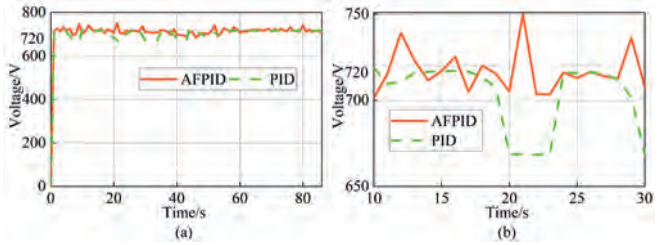

Fig. 15. (a) The bus voltage; (b) The bus voltage between 10s and 30s

CONCLUSIONS

In this paper, the EMS with hierarchical control is presented. In addition, an ESS degradation model is developed to assess the ESS SOH and reduce capacity loss. The key findings can be summarized as below:

(i) The FCS output power is constant or increases slowly with the PSO-ECMS. Compared to the SVM-based EMS, the output power curve of the FCS is smoother and the hydrogen consumption reduces by 5.319% without considering ESS degradation during the entire operation.

(ii) The AFPID controller can adjust the three parameters of PID in real time according to the change in the system state. Compared to the conventional PID controller, the bus voltage fluctuation is smaller and the bus voltage can be restored to the reference value within a shorter time when the load changes suddenly. The dynamic and static performance of the shipboard power system is significantly improved.

(iii) An ESS degradation model is developed to calculate the capacity loss. Although hydrogen consumption has increased, the total operating cost reduces by 1.7% after adding the capacity loss to the objective function.

REFERENCES

1. Z. Korczewski, "Test method for determining the chemical emissions of a marine diesel engine exhaust in operation," *Polish Maritime Research*, 2021. doi:10.2478/pomr-2021-0035.

2. M. Barakat, B. Tala-Ighil, H. Chaoui, H. Gualous, D. Hissel, "Energy Management of a Hybrid Tidal Turbine-Hydrogen Micro-Grid: Losses Minimization Strategy," *Fuel Cells*, 2020. doi:10.1002/fuce.201900082.

3. P. Geng, X. Y. Xu, T. Tarasiuk, "State of charge estimation method for lithium-ion batteries in all-electric ships based on LSTM neural network," *Polish Maritime Research*, 2020. doi:10.2478/pomr-2020-0051.

4. R. Zhao *et al.*, "A numerical and experimental study of marine hydrogen-natural gas-diesel trifuel engines," *Polish Maritime Research*, 2020. doi:10.2478/pomr-2020-0068.

5. M. Rafiei, J. Boudjadar, M. H. Khooban, "Energy Management of a Zero-Emission Ferry Boat With a Fuel-Cell-Based Hybrid Energy System: Feasibility Assessment," *IEEE Trans. Ind. Electron.*, 2021. doi:10.1109/tie.2020.2992005.

6. S. Faddel, A. A. Saad, M. E. Hariri, O. A. Mohammed, "Coordination of Hybrid Energy Storage for Ship Power Systems With Pulsed Loads," *IEEE Trans. Ind. Appl.*, 2020. doi:10.1109/tia.2019.2958293.

7. S. Hasanvand, M. Rafiei, M. Gheisarnejad, M. H. Khooban, "Reliable Power Scheduling of an Emission-Free Ship: Multiobjective Deep Reinforcement Learning," *IEEE Trans. Transport. Electrif.*, 2020. doi:10.1109/tte.2020.2983247.

8. P. Wu, J. Partridge, R. Bucknall, "Cost-effective reinforcement learning energy management for plug-in hybrid fuel cell and battery ships," *Applied Energy*, 2020. doi:10.1016/j.apenergy.2020.115258.

9. M. Banaei, J. Boudjadar, M. H. Khooban, "Stochastic Model Predictive Energy Management in Hybrid Emission-Free Modern Maritime Vessels," *IEEE Trans. Ind. Inform.*, 2021. doi:10.1109/tii.2020.3027808.

10. J. Hou, Z. Y. Song, H. Hofmann, J. Sun, "Adaptive model predictive control for hybrid energy storage energy management in all-electric ship microgrids," *Energy Conversion and Management*, 2019. doi:10.1016/j.enconman.2019.111929.

11. M. Banaei, M. Rafiei, J. Boudjadar, M. H. Khooban, "A Comparative Analysis of Optimal Operation Scenarios in Hybrid Emission-Free Ferry Ships," *IEEE Trans. Transport. Electrif.*, 2020. doi:10.1109/tte.2020.2970674.

12. J. Nunez Forestieri, M. Farasat, "Energy flow control and sizing of a hybrid battery/supercapacitor storage in MVDC shipboard power systems," *IET Electrical Systems in Transportation*, 2020. doi:10.1049/iet-est.2019.0161.

13. M. H. Khooban, M. Gheisarnejad, H. Farsizadeh, A. Masoudian, J. Boudjadar, "A New Intelligent Hybrid Control Approach for DC-DC Converters in Zero-Emission Ferry Ships," *IEEE Trans. Power. Electron.*, 2020. doi:10.1109/tpel.2019.2951183.

14. T. H. Wang *et al.*, "A Power Allocation Method for Multistack PEMFC System Considering Fuel Cell Performance Consistency," *IEEE Trans. Ind. Appl.*, 2020. doi:10.1109/tia.2020.3001254.

15. J. Chen, C. Xu, C. Wu, W. Xu, "Adaptive Fuzzy Logic Control of Fuel-Cell-Battery Hybrid Systems for Electric Vehicles," *IEEE Trans. Ind. Inform.*, 2018. doi:10.1109/tii.2016.2618886.

16. F. Balsamo, P. De Falco, F. Mottola, M. Pagano, "Power Flow Approach for Modeling Shipboard Power System in Presence of Energy Storage and Energy Management Systems," *IEEE Trans. Energy Convers.*, 2020. doi:10.1109/tec.2020.2997307.

17. H. Ahmadi, M. Rafiei, M. A. Igder, M. Gheisarnejad, M. H. Khooban, "An Energy Efficient Solution for Fuel Cell Heat Recovery in Zero-Emission Ferry Boats: Deep Deterministic Policy Gradient," *IEEE Trans. Veh. Technol.*, 2021. doi:10.1109/tvt.2021.3094899.

18. [18] A. Boveri, F. Silvestro, M. Molinas, E. Skjong. Optimal Sizing of Energy Storage Systems for Shipboard Applications. *IEEE Trans. Energy Convers.* 2019. doi:10.1109/TEC.2018.2882147.

19. Y. Z. Zhang *et al.*, "Real-Time Energy Management Strategy for Fuel Cell Range Extender Vehicles Based on Nonlinear Control," *IEEE Trans. Transport. Electrif.*, 2019. doi:10.1109/tte.2019.2958038.

20. C. Lin, H. Mu, R. Xiong, W. X. Shen, "A novel multi-model probability battery state of charge estimation approach for electric vehicles using H-infinity algorithm," *Applied Energy*, 2016. doi:10.1016/j.apenergy.2016.01.010.

21. X. Y. Lu, H. Y. Wang, "Optimal Sizing and Energy Management for Cost-Effective PEV Hybrid Energy Storage Systems," *IEEE Trans. Ind. Inform.*, 2020. doi:10.1109/tii.2019.2957297.

22. J. Park *et al.*, "Semi-empirical long-term cycle life model coupled with an electrolyte depletion function for large-format graphite/LiFePO4 lithium-ion batteries," *Journal of Power Sources*, 2017. doi:10.1016/j.jpowsour.2017.08.094.

23. J. Wang *et al.*, "Cycle-life model for graphite-LiFePO4 cells," *Journal of Power Sources*, 2011. doi:10.1016/j.jpowsour.2010.11.134.

24. M. Kalikatzarakis, R. D. Geertsma, E. J. Boonen, K. Visser, R. R. Negenborn, "Ship energy management for hybrid propulsion and power supply with shore charging," *Control Engineering Practice*, 2018. doi:10.1016/j.conengprac.2018.04.009.

25. H. Chen, Z. H. Zhang, C. Guan, H. B. Gao, "Optimization of sizing and frequency control in battery/supercapacitor hybrid energy storage system for fuel cell ship," *Energy*, 2020. doi:10.1016/j.energy.2020.117285.